Supplementary Information for "Structural warming biases distort extreme rainfall intensification estimates in event attribution"

Damián Insua-Costa[1], Marc Lemus-Cánovas[2], Martín Senande-Rivera[3], Victoria M. H. Deman[1], João L. Geirinhas[1], and Diego G. Miralles[1]

[1]Hydro-Climate Extremes Lab, Ghent University, 9000 Ghent, Belgium
[2]Center for Climate Change and Transformation, Eurac Research, 39100 Bolzano/Bozen, Italy
[3]Mitiga Solutions, 08002 Barcelona, Spain
Correspondence: damian.insuacosta@ugent.be

Table S1. Information on the six CMIP6 models used in the study, including developing institution, country, atmospheric horizontal resolution, and local warming signal. The warming signal (°C) corresponds to the near-surface warming over the city of Valencia derived using the annual-mean delta approach (2009–2039 minus 1850–1880); it is reported to illustrate the spread in the perturbations used in our Valencia attribution experiments.

Model	Institution	Country	Resolution	Warming (°C)
BCC-CSM2-MR	Beijing Climate Center (BCC)	China	$\sim 1.125^\circ \times 1.125^\circ$	1.76
CESM2-WACCM	National Center for Atmospheric Research (NCAR)	USA	$\sim 1.25^\circ \times 0.9^\circ$	1.31
EC-Earth3	EC-Earth Consortium	Europe	$\sim 0.7^\circ \times 0.7^\circ$	1.26
GFDL-ESM4	NOAA Geophysical Fluid Dynamics Laboratory (GFDL)	USA	$\sim 1.0^\circ \times 1.0^\circ$	1.01
MPI-ESM1-2-HR	Max Planck Institute for Meteorology (MPI-M)	Germany	$\sim 0.94^\circ \times 0.94^\circ$	1.63
MRI-ESM2-0	Meteorological Research Institute (MRI)	Japan	$\sim 1.125^\circ \times 1.125^\circ$	1.54

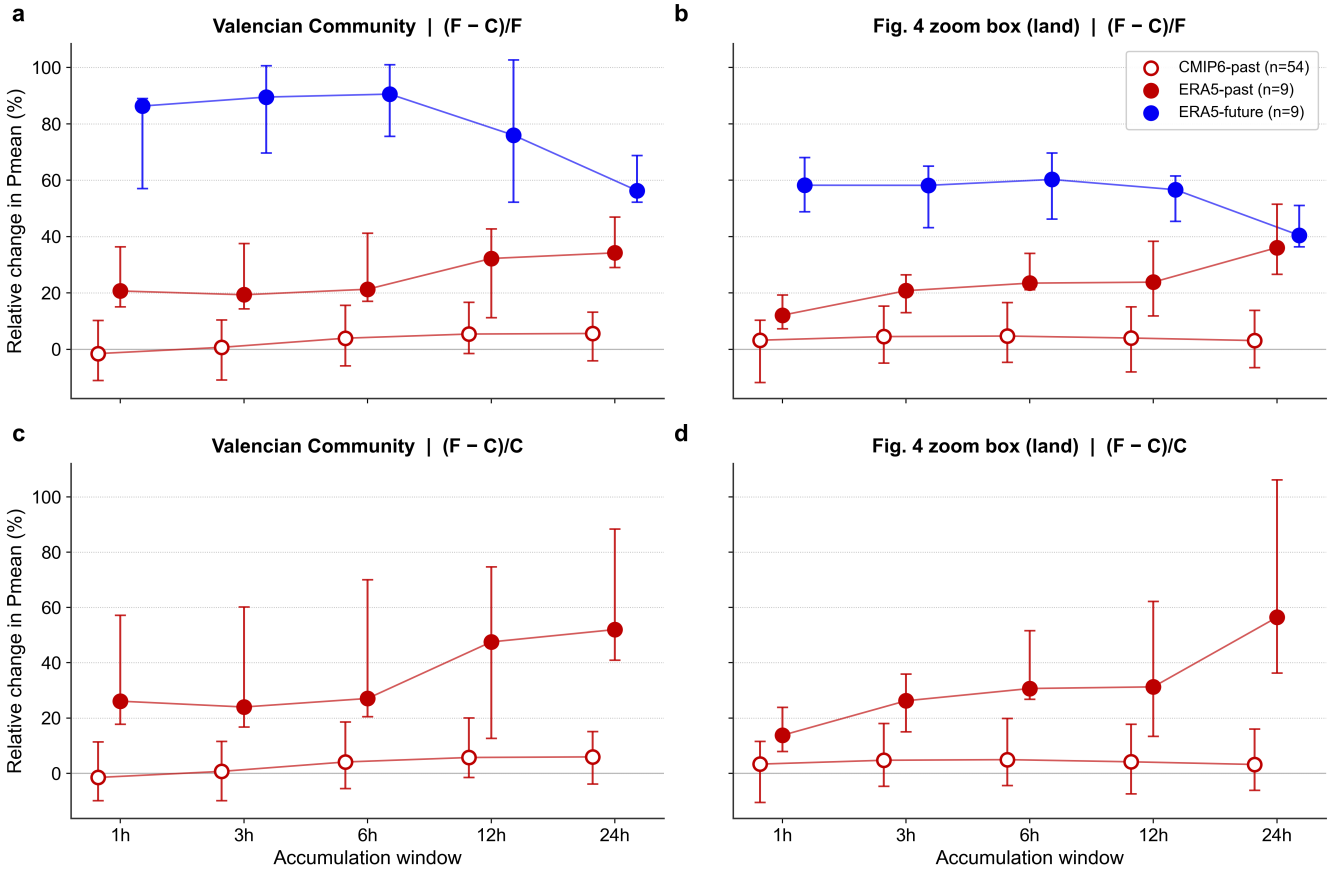

Figure S1. Sensitivity of attribution outcomes to (i) the accumulation window of the precipitation metric, (ii) the spatial mask, and (iii) the choice of normalisation in the delta percentage. Markers show median values and error bars show the IQR for each ensemble (CMIP6-past, $n = 54$; ERA5-past, $n = 9$; ERA5-future, $n = 9$). The top row uses the formulation $(F - C)/F$ (consistent with the main text) and the bottom row uses $(F - C)/C$. The left column uses the Valencian Community mask (same as Fig. 5) and the right column uses the land portion of the Fig. 4 zoom box. For the ERA5-future ensemble the numerator is inverted to $(C - F)/F$ so that the metric represents the intensification of the response under future warming. This ensemble appears only under $(F - C)/F$, since the $(F - C)/C$ normalisation is meaningful only when C is the colder counterfactual.

Figure S2. Unstructured grid used in all MPAS simulations, characterised by variable horizontal resolution ranging from 60 km to 3 km. The high-resolution zone (darker) is centred over the western Mediterranean.

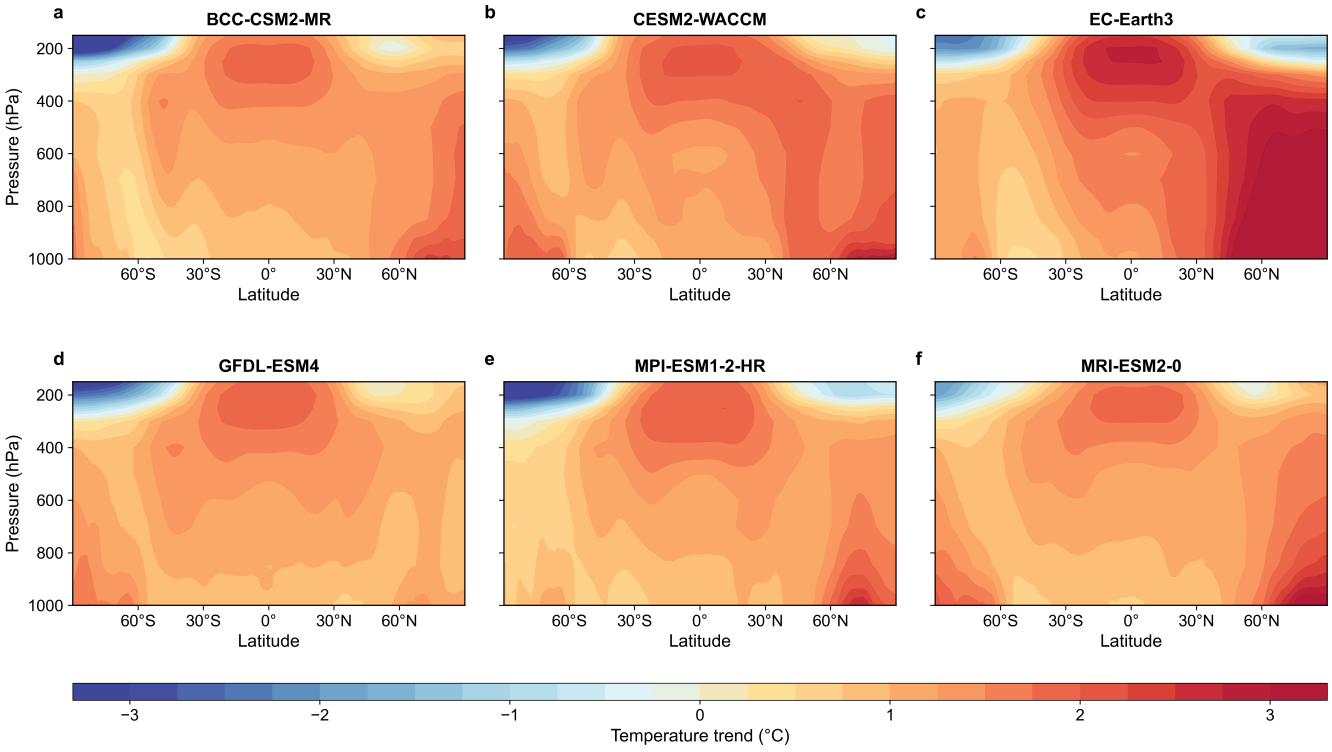

Figure S3. Zonal-mean air-temperature trends from six CMIP6 models. Trends are calculated from annual-mean temperatures over 1940–2024 at standard pressure levels between 1000 and 150 hPa, expressed as the total warming over the 85-year period (°C). All six models reproduce a similar zonal-mean structure, with two clear warming maxima—one over the Arctic and another in the tropical upper troposphere—consistent with the multi-model mean shown in Fig. 1 of the main text.

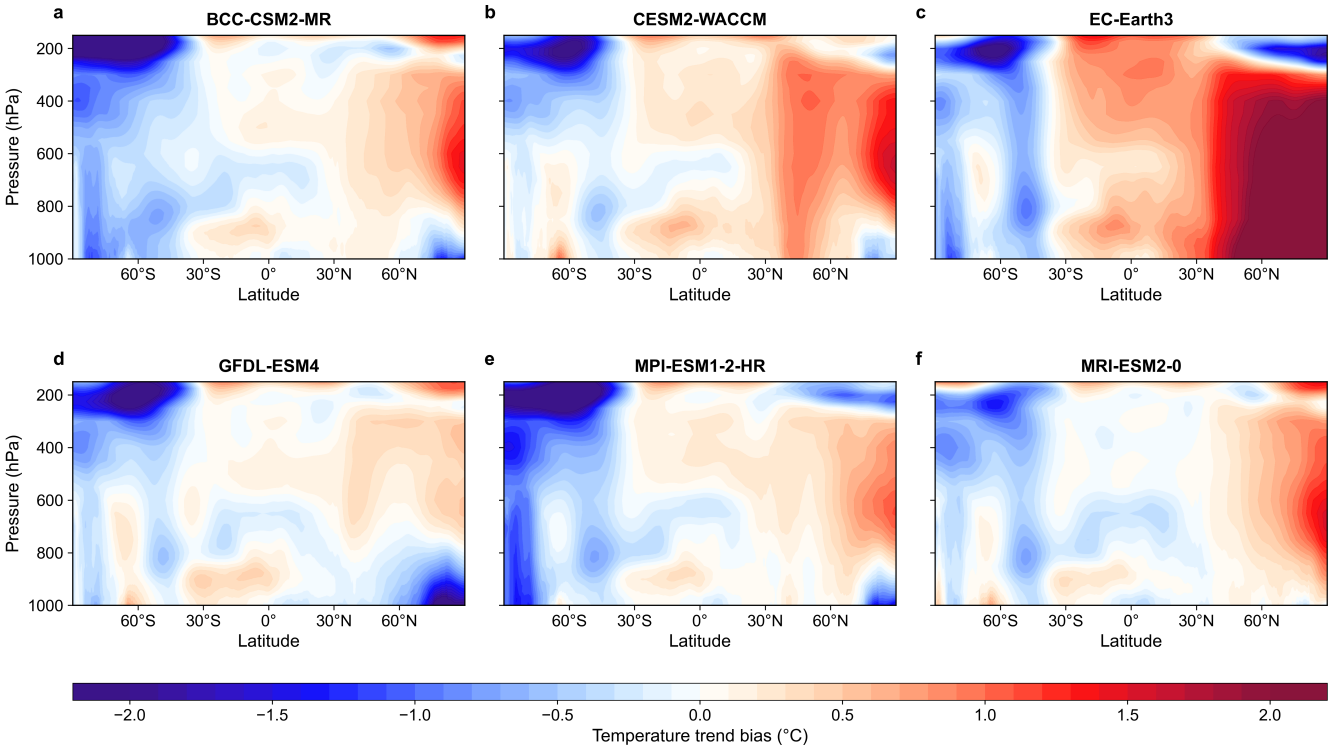

Figure S4. Difference between CMIP6 and ERA5 in zonal-mean air-temperature trends for the six CMIP6 models used in the study. Trends are calculated from annual-mean temperatures over 1940–2024 at standard pressure levels between 1000 and 150 hPa, expressed as the total warming over the 85-year period (°C). The model-to-model spread is small compared with the systematic CMIP6−ERA5 bias, indicating that the structural mismatch identified in the main text is robust across the model subset.

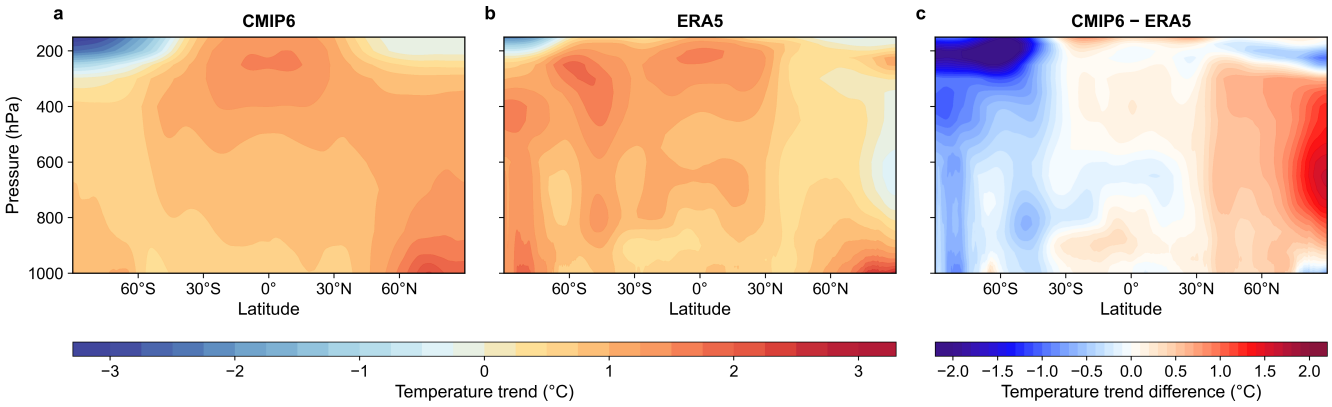

Figure S5. Zonal-mean air-temperature trends at standard pressure levels between 1000 and 150 hPa from the CMIP6 multi-model mean (a), ERA5 (b), and the CMIP6−ERA5 difference (c). The figure is identical to Fig. 1 of the main text, except that trends are calculated from annual-mean temperatures over 1940–2014 (°C/75 years) rather than 1940–2024. Restricting the comparison to the common historical-only period demonstrates that the spatial patterns and biases identified are robust to the inclusion of the 2015–2024 SSP2-4.5 segment in CMIP6.

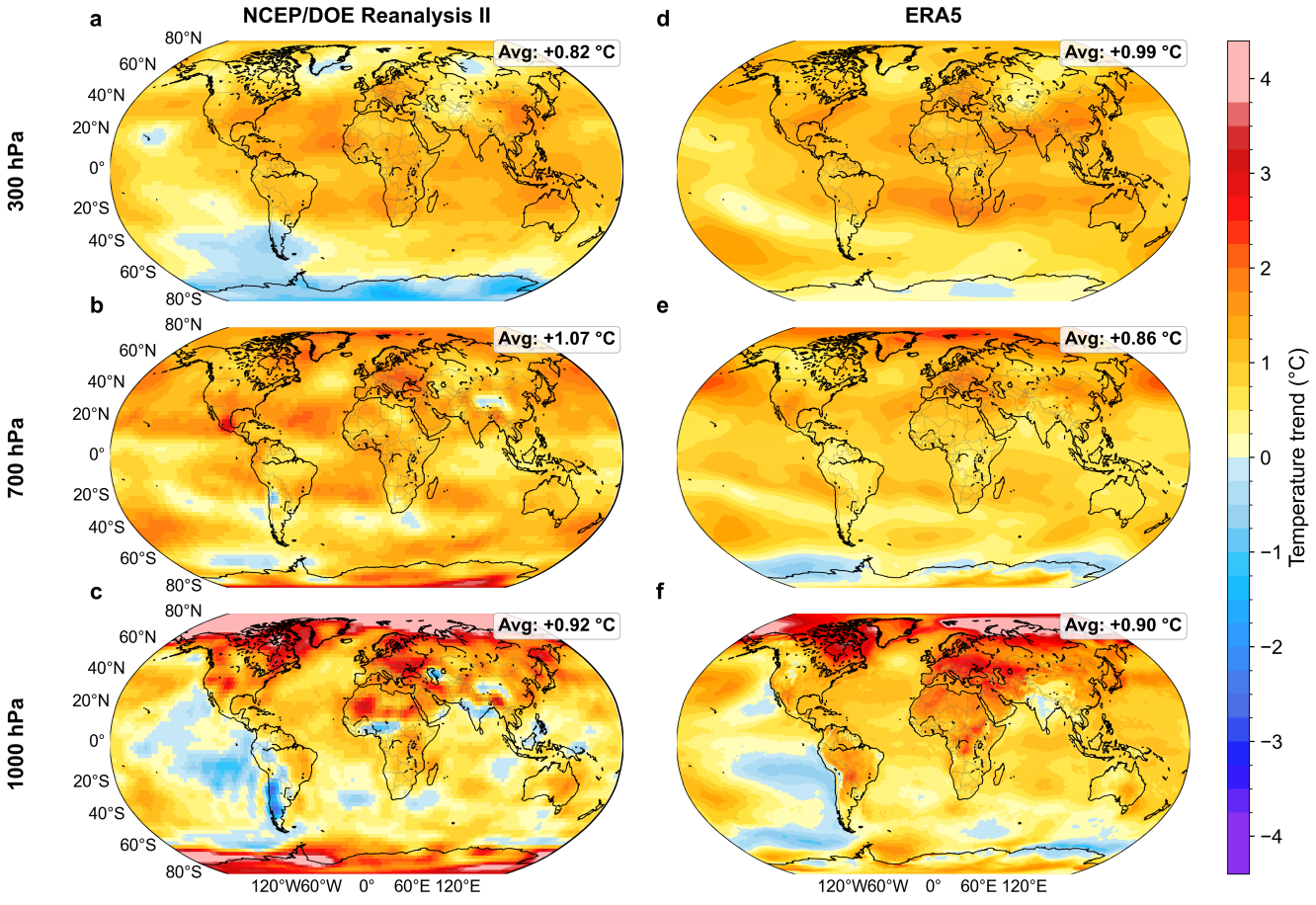

Figure S6. Air-temperature trends from the NCEP/DOE Reanalysis II (a, b, c) and ERA5 (d, e, f) at 300, 700 and 1000 hPa. Global-mean trends for each panel are shown in the upper-right corners of the maps. Values correspond to linear trends in annual-mean temperature over 1979–2024 (°C/46 years). Note that the period differs from that in Fig. 2 of the main text (1940–2024) because the NCEP/DOE Reanalysis II begins in 1979 and a common period is required for comparison.

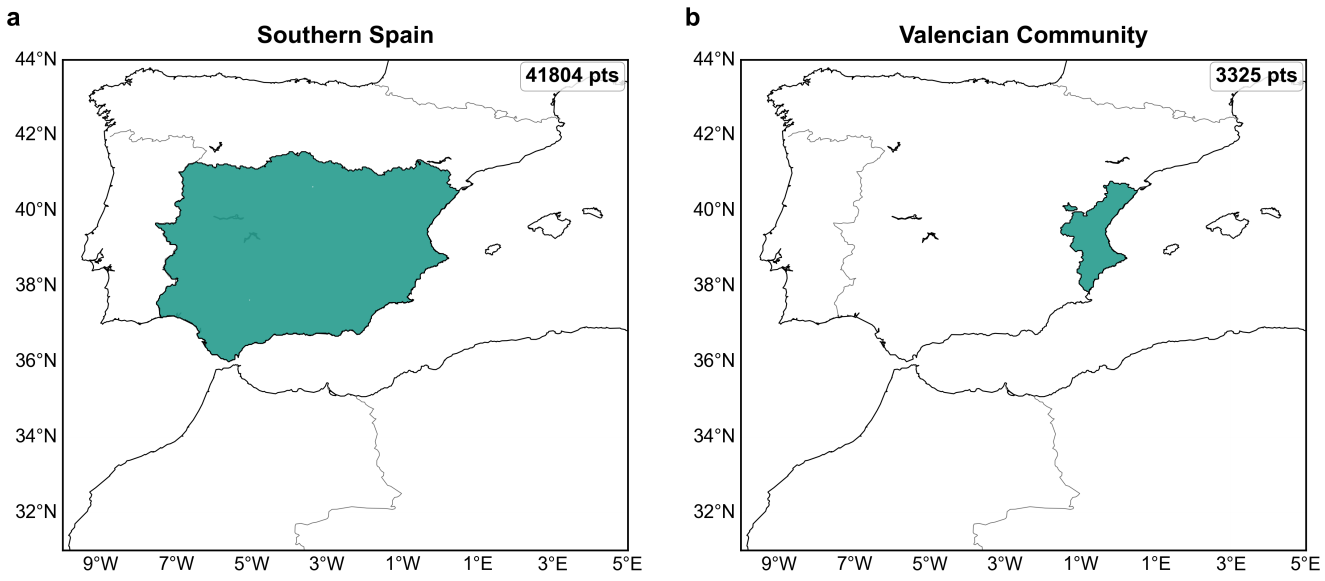

Figure S7. Southern Spain (a) and the Valencian Community (b), the two integration domains referenced throughout the study. The larger region encompasses approximately the entire area affected by the event, whereas the Valencian Community corresponds to the area most strongly impacted by extreme precipitation (Fig. 4d, e, f of the main text). Boxplots in Fig. 5 of the main text use the Valencian Community, while boxplots in Fig. S8 use the Southern Spain domain.

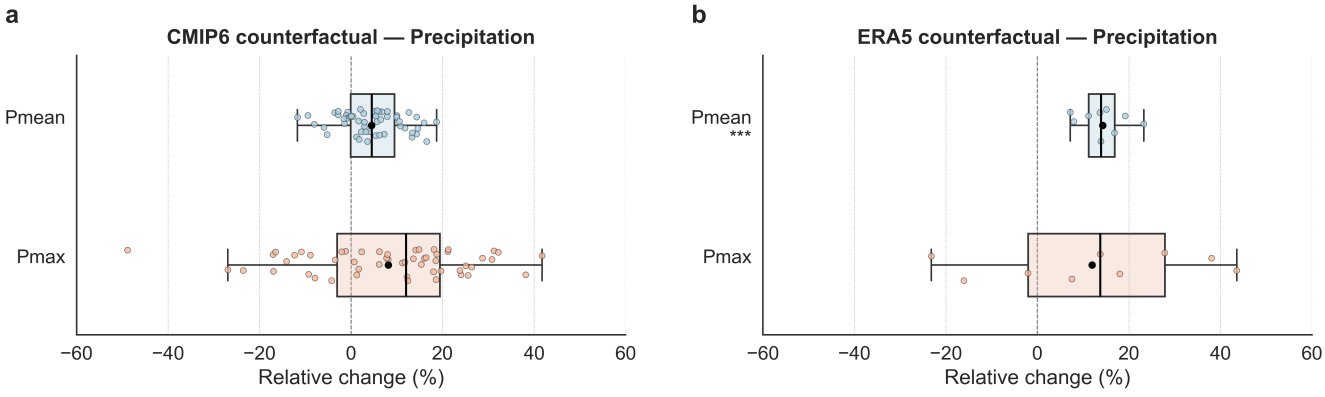

Figure S8. Relative differences in mean and maximum 24-h precipitation between the factual and CMIP6-past counterfactual ensembles (a) and between the factual and ERA5-past counterfactual ensembles (b), expressed as $(F - C)/F \times 100$, with Southern Spain (Fig. S7a) as the integration domain instead of the Valencian Community used in Fig. 5 of the main text. Asterisks denote statistical significance as in Fig. 5.

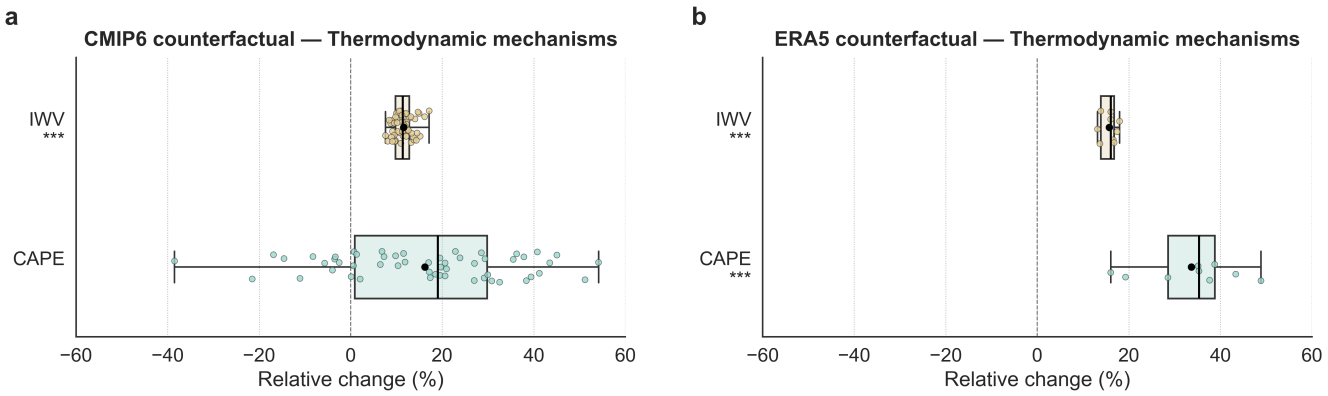

Figure S9. Relative differences in integrated water vapour (IWV) and convective available potential energy (CAPE) between the factual and counterfactual ensembles (CMIP6-past, a; ERA5-past, b), expressed as $(F - C)/F \times 100$. Values correspond to 06:00 UTC on 29 October 2024, rather than daily means for that day as in Fig. 5 of the main text. This pre-convective sampling emphasises the thermodynamic preconditioning of the atmosphere prior to the main convective phase.

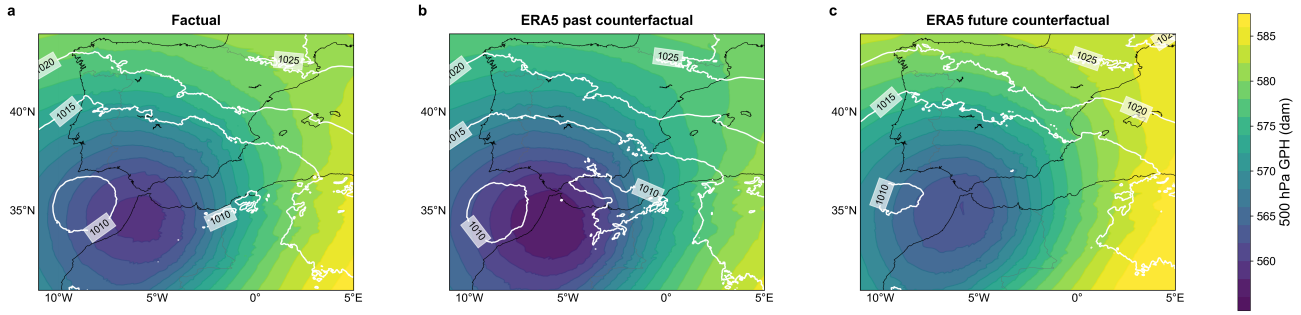

Figure S10. Mean 500-hPa geopotential height (colours, dam) and sea-level pressure (white contours, hPa) at 12 UTC on 29 October 2024 for the factual ensemble (a), the ERA5-past counterfactual (b), and the ERA5-future counterfactual (c). Same fields and convention as the top row of Fig. 4 of the main text, here extended with the future case.